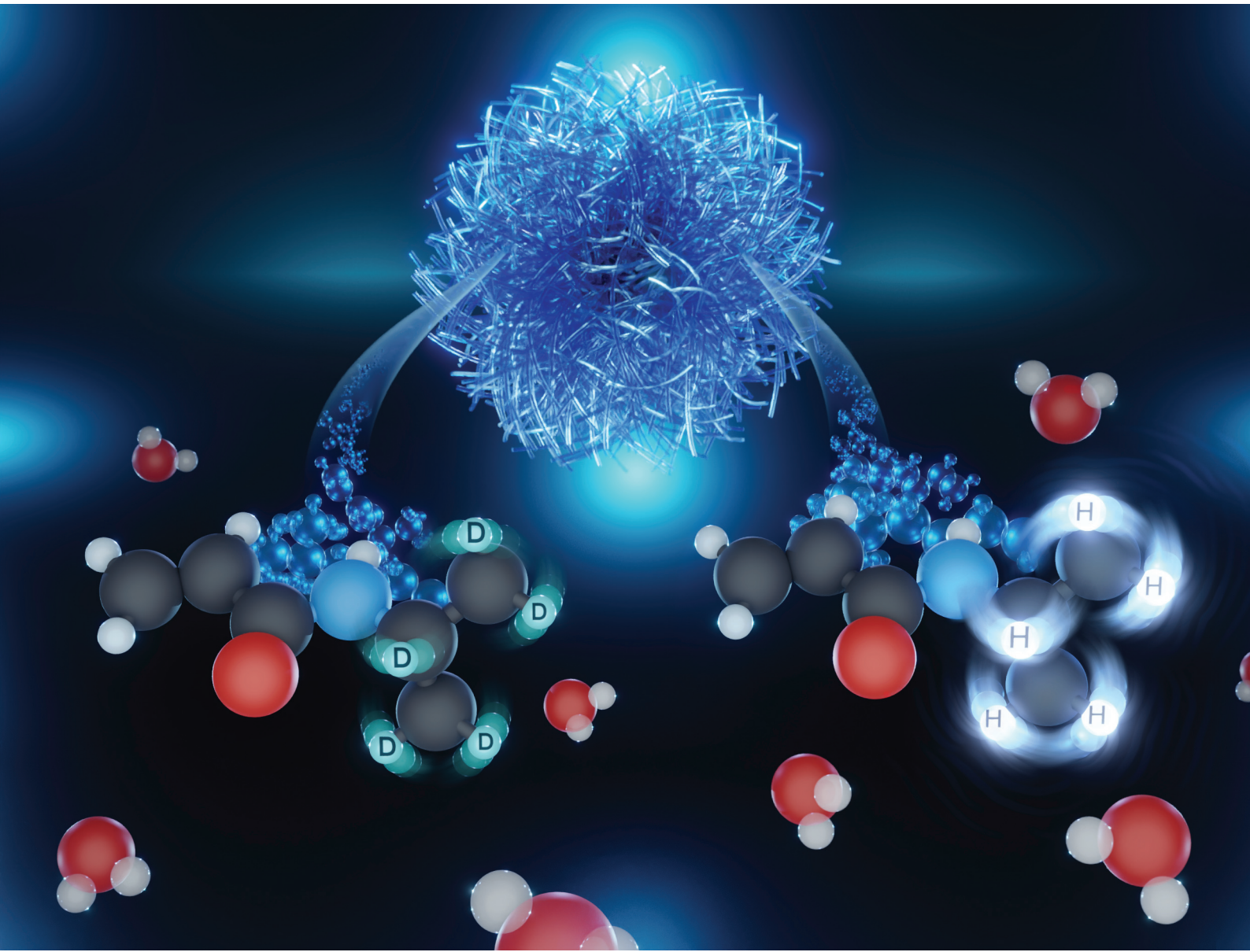


# Polymer Chemistry

[rsc.li/polymers](https://rsc.li/polymers)



ISSN 1759-9962

**PAPER**

Andrea Scotti, Kai Leonhard *et al.*  
Understanding the monomer deuteration effect on the  
transition temperature of poly(*N*-isopropylacrylamide)  
microgels in H<sub>2</sub>O



Cite this: *Polym. Chem.*, 2023, **14**, 1447

## Understanding the monomer deuteration effect on the transition temperature of poly(*N*-isopropylacrylamide) microgels in H<sub>2</sub>O†

Thomas Nevolianis, <sup>a</sup> Andrea Scotti, <sup>\*b</sup> Alexander V. Petrunin, <sup>b</sup> Walter Richtering <sup>b</sup> and Kai Leonhard <sup>\*a</sup>

Obtaining deuterated micro- and nanogels is essential to characterize their architecture and determine their response to crowding using neutron scattering with contrast variation. Experimental studies have reported that deuterated microgels have a higher volume phase transition temperature (VPTT) than hydrogenated microgels. However, to date, the effect of deuteration on the microgel properties has yet to be fully understood, questioning whether deuterated and hydrogenated microgels have comparable responsiveness to external stimuli, structure, and compressibility. To answer these questions, we both simulate and measure the effect of deuteration on the VPTT of *N*-isopropylacrylamide (NIPAM)-based microgels. Using quantum mechanical methods and considering only the zero-point energy difference, we study different NIPAM-(H<sub>2</sub>O)<sub>n</sub> complexes and calculate the changes in the value of the Flory interaction parameter as a consequence of deuteration. The resulting interaction parameter is used in the Flory–Rehner theory to predict microgels' swelling behavior. Using multi-angle dynamic light scattering, we measure the hydrodynamic radius of non- and deuterated microgels as a function of temperature. Based on our model results, we obtain a VPTT shift of 4.9 K, only due to the zero-point energy difference between complexes containing H<sub>2</sub>O and NIPAM/D<sub>n</sub>NIPAM, which agrees with the 4.3 K shift of the VPTT observed in the experiments. In the future, our approach may be used to adjust effective parameters in molecular dynamics simulations studying deuterated microgels and providing insights into their properties, including VPTT, swelling ratio, and softness.

Received 30th November 2022,  
Accepted 31st January 2023

DOI: 10.1039/d2py01511k  
[rsc.li/polymers](http://rsc.li/polymers)

## 1 Introduction

The use of colloidal systems to study phase transitions and the flow properties of complex fluids is pivotal to both advance the understanding of fundamental problems<sup>1,2</sup> and developing soft materials for industrial applications.<sup>3</sup> In the last decades, the effects of softness on the self-assembly and macroscopic properties of soft materials have been largely investigated using micro- and nanogels.<sup>4</sup> These particles consist of a cross-linked polymeric network, which contains up to >90% solvent in their swollen state.<sup>5–8</sup> Consequently, these colloids are soft and deformable and can respond to increases of concentration in solution with both isotropic deswelling or faceting.<sup>9–12</sup> Furthermore, if the polymer used in the synthesis is stimuli-

responsive, the obtained particles are responsive to changes in the environments.<sup>3</sup> For instance, poly(*N*-isopropylacrylamide) (NIPAM)-based microgels in H<sub>2</sub>O are thermoresponsive since the pNIPAM has a lower critical solution temperature (LCST).<sup>13,14</sup> Below 305 K, H<sub>2</sub>O is a good solvent and the microgels are swollen and soft. Above this temperature, there is a volume phase transition and the H<sub>2</sub>O content decreases, making the microgel more compact and similar to a hard colloid.<sup>5</sup> This property is appealing for both application and fundamental research. Microgels allow to realize responsive smart materials such as membranes for H<sub>2</sub>O filtration,<sup>15</sup> responsive emulsions,<sup>16</sup> and nano-carriers for drug delivery.<sup>17</sup> The possibility of the microgels to change their volume in solution simply by changing the sample temperature also allows to explore the sample properties as a function of crowding in crystals, glasses, or jammed phases.<sup>18–23</sup>

To appropriately tailor the microgel properties for applications and correctly interpret their behavior when used as models for atomic systems, one must adequately characterize their architecture and the changes in their structure due to the changes in their external environment. For these applications,

<sup>a</sup>Institute of Technical Thermodynamics, RWTH Aachen University, 52062 Aachen, European Union, Germany. E-mail: kai.leonhard@ltt.rwth-aachen.de

<sup>b</sup>Institute of Physical Chemistry, RWTH Aachen University, 52056 Aachen, European Union, Germany. E-mail: scotti@pc.rwth-aachen.de

† Electronic supplementary information (ESI) available. See DOI: <https://doi.org/10.1039/d2py01511k>

the size of the microgels cannot exceed a few hundred nanometers. Therefore, scattering techniques are the only option to characterize such properties. In particular, small-angle neutron scattering with contrast variation is an advanced technique to investigate functional polymers as it allows us to selectively isolate and study the samples' parts.<sup>6,9,24–29</sup> This is because neutrons can distinguish between hydrogen and deuterium since they interact with the nuclei of the atoms composing the samples and not with their electron clouds.<sup>30</sup> The use of deuterated monomers during the synthesis can result either in partially deuterated microgels or in individual microgels with regions composed of partially deuterated polymer. In both cases, a mixture of H<sub>2</sub>O and D<sub>2</sub>O can be used to selectively mask the deuterated or protonated part of the sample.<sup>31</sup> This approach has been successfully used to characterize specific regions in the microgels<sup>6,28,32,33</sup> or study the response of individual microgels to crowding.<sup>9,24–27</sup>

However, it has to be taken into account that deuteration can influence the reactivity of monomers and thus structure–property relationships of polymers might be affected. A recently reported example concerns the softest NIPAM-based microgels that can be realized by precipitation polymerization, which are the so-called ultra-low crosslinked microgels.<sup>4,34</sup> These particles are synthesized without adding a crosslinker agent, and the polymeric network forms due to the NIPAM self-crosslinking.<sup>34</sup> However, they cannot be synthesized using the usual deuterated monomer with seven deuterium atoms. This is because the isopropyl group of NIPAM is deuterated. A NIPAM deuterated monomer with only three deuterium atoms in the monomer backbone has been successfully used. We note that the deuterated and regular ultra-low crosslinked microgels have similar properties compared to regular microgels and microgels synthesized using the pD-NIPAM. For instance, they show a closer swelling ratio, *i.e.*, softness,<sup>4</sup> and the shift of the VPTT due to deuteration is negligible within the experimental error (see ESI†).

A key question is whether or not the use of a deuterated monomer changes the properties of the microgels. For instance, microgels synthesized using NIPAM with the seven hydrogen atoms of the isopropyl group substituted by deuterium show a higher VPTT compared to microgels synthesized using [C<sub>6</sub>H<sub>11</sub>NO]<sup>34,35</sup>

Furthermore, the use of this deuterated monomer suppresses the self-crosslinking<sup>34</sup> and leads to obtaining microgels with a slightly different internal architecture compared to the one synthesized with the fully hydrogenated monomer.<sup>6</sup> This means that selective deuteration might affect both the swelling behaviour and the internal structure and amount of crosslinking of the microgels. A possibility to compensate for the absence of self-crosslinking is to use a slightly different amount of crosslinker during the synthesis of deuterated and hydrogenated microgel to achieve a similar swelling ratio of the particles.<sup>26,27</sup> However, this might as well affect the internal architecture of the microgel. As we have recently shown, the softness of a particle can be defined in various ways and depends on many aspects such as swelling degree,

internal architecture, and elastic moduli.<sup>4</sup> Therefore, the fact that deuterated and hydrogenated microgels have a comparable swelling ratio cannot guarantee *per se* that the two microgel have the same softness and a more detailed understanding of the deuteration effects on the microgel synthesis is needed.

Another aspect that must be considered is that selective deuteration changes the interaction between solvent and polymer.<sup>36</sup> It is well known that both the use of deuterated solvents and selective deuteration change the VPTT of pNIPAM.<sup>37</sup> The thermodynamics governing the microgel swelling has been described using the Flory–Huggins model.<sup>38–40</sup> For neutral microgels, such as the pNIPAM ones, the swelling equilibrium is determined by the balance between the free energy due to the solvent–polymer mixing and the elasticity of the crosslinked polymeric network. Using this mean-field approach, microgels have been approximated by combining the Flory–Rehner theory of swelling of crosslinked polymer networks<sup>41–43</sup> with the Hertz theory of pair interactions between elastic bodies.<sup>44</sup> Many studies<sup>45–47</sup> report values of Flory–Rehner theory's parameters in different ranges by describing successfully the swelling curve of microgels and thus, these parameter values vary and their choice is debatable.<sup>48</sup>

Since our main focus here is to study the deuteration effect of pNIPAM microgels at a fundamental level of theory and therefore, the choice of the parameters, as long as they still have a physical meaning, is not relevant. Approaches such as Monte Carlo simulations based on the Flory–Hertz model of microgels have been primarily used to describe the response of microgels to crowding.<sup>24,38,40</sup> Different mechanistic models<sup>49–52</sup> with quantum mechanical estimated parameters<sup>53–56</sup> have been used to model microgel synthesis and tailor new microgel functionalities. New challenges appear for interpreting the swelling behavior of deuterated microgels due to interactions that the above-mentioned macroscopic models can not capture.

Thermoresponsivity of polymers in aqueous solution is governed by the interaction of the macromolecule with the solvent water. In this scenario, quantum mechanical calculations can provide unique information on the microscopic interactions between the solvent and deuterium substituted atoms and thus provides new insight in designing (partially) deuterated monomers to tailor properties of thermoresponsive polymers. In contrast to classical mechanics, nuclei show nuclear quantum effects such as zero-point energy, which are more pronounced for lighter isotopes.<sup>57</sup> Detailed studies on isotope effects using different approaches can be found in the literature.<sup>58–60</sup> Using quantum mechanical calculations, studies have successfully investigated equilibrium isotope effects of supramolecular host–guest systems<sup>61</sup> and pyridine.<sup>62</sup> In the case of microgels, quantum mechanic calculations can be used to study the effect of deuteration by considering only the zero-point energy difference and predicting the change of the Flory interaction parameter upon deuteration, which then can be used in the Flory–Rehner theory to model the swelling behavior of deuterated microgels.

Among the different deuterated monomers of NIPAM, the most commonly used one to realize partially or fully deuterated microgels is the one with seven deuterium atoms. Partially deuterated and fully deuterated pD<sub>7</sub>NIPAM microgels have mainly been used to determine the individual particle shape both in diluted,<sup>32,33,37</sup> and concentrated suspensions.<sup>4,24–27,63</sup> For these microgels, a single monomer is a promising model for studying the effect of deuteration. Given the large shifts in the VPTT, the different swelling ratios, and the large use of D<sub>7</sub>NIPAM, this monomer will be the main focus of this study. For another used NIPAM deuterated monomer, the D<sub>3</sub>NIPAM, such a single monomer approach seems less promising since the backbone atoms are in different hybridization states in the monomer (sp<sup>2</sup>) and the polymer (sp<sup>3</sup>), leading to different interactions with their environment. In addition, it is known that small changes in the precise backbone structure can have large effects on the VPTT of polymers, *e.g.*, adding a methyl group to the backbone of pNIPAM counter-intuitively increases the VPTT.<sup>64</sup> Therefore, a single monomer cannot be used as a model molecule, making quantum mechanical calculations orders of magnitude more expensive than for pD<sub>7</sub>NIPAM. However, as we mentioned above, the use of this monomer seems to have a negligible effect on the swelling properties, and VPTT shift of the obtained microgels compared with NIPAM-based ultra-low crosslinked microgels and, therefore, small changes on the quantum-mechanic scales are expected.

All quantum mechanical studies of the effect of deuteration we are aware of have studied the deuteration of solutes, not of the solvent, see, *e.g.*, ref. 61 and 62. It turned out that an extension of their approach to the deuteration of the solvent is not easily possible (see ESI† for more details). Therefore, the changes in the VPTT of hydrogenated (C<sub>6</sub>H<sub>11</sub>NO) and partially deuterated (C<sub>6</sub>H<sub>4</sub>D<sub>7</sub>NO) NIPAM-based microgels suspended in H<sub>2</sub>O are investigated. In this study, the D<sub>7</sub>NIPAM microgel is used as an example to study the deuteration effect due to its large VPTT shift. We calculate the change of the Flory interaction parameter upon deuteration using quantum mechanical methods and considering only the zero-point energy difference. The results are used to model the swelling curve of the deuterated microgel, and the model predictions are validated against experimental observations. Different vibrational modes of NIPAM and D<sub>7</sub>NIPAM with H<sub>2</sub>O result in a difference in zero-point energy (ZPE). This difference influences the Flory interaction parameter and leads to the VPTT shift.

## 2 Materials and methods

### 2.1 Synthesis

All the microgels used in this study are obtained by standard precipitation polymerization. The main monomer used is *N*-isopropylacrylamide (NIPAM) ([C<sub>6</sub>H<sub>11</sub>NO]<sub>n</sub>) or deuterated monomers of NIPAM in which the seven hydrogen atoms of the isopropyl group have been substituted by deuterium. The ratio between the crosslinker *N,N'*-methylenebisacrylamide

(BIS) and the monomer is 5 mol% in all the synthesis. The syntheses were performed according to standard precipitation polymerization.<sup>5,14</sup> Surfactants have also been added during the synthesis to control the final microgel size and the size polydispersity.<sup>65</sup> All samples were prepared using bi-distilled Milli-Q H<sub>2</sub>O as a solvent. A detailed description of the synthesis procedure for these microgels can be found in the literature.<sup>24</sup>

### 2.2 Dynamic light scattering

Multi-angle dynamic light scattering (DLS) was used to measure the intensity autocorrelation functions of diluted suspensions of microgels. The light source was a laser with a wavelength in vacuum  $\lambda_0 = 633$  nm. The refractive index of the H<sub>2</sub>O was  $n(\lambda_0) = 1.33$ . The scattering vector is defined as  $q = 4\pi n/\lambda_0 \sin(\theta/2)$  and it was changed using scattering angles  $\theta$  between 30° and 110° with steps of 10°. The solutions of microgels have been measured at a temperature between 293 K and 323 K in steps of 2 K. A thermal bath filled with toluene to match the refractive index of the glass was used to control the temperature during the measurements.

From the analysis of the intensity autocorrelation functions with the second-order cumulant method,<sup>66</sup> the decay rates,  $\Gamma$ , were obtained for each  $q$ -value.<sup>67,68</sup> The errors on the values of  $D_0$  are computed using a linear regression.<sup>68</sup> Finally, the value of the hydrodynamic radius,  $R_H$ , was obtained using the Stokes–Einstein equation:  $R_H = k_B T / (6\pi\eta\Gamma(T)D_0)$ , where  $\eta(T)$  is the viscosity of the solvent used at the temperature  $T$  and  $k_B$  is the Boltzmann's constant. The errors on the values of  $R_H$  are obtained from error propagation of the uncertainty on  $D_0$  and  $T$  ( $\pm 0.1$  K).

### 2.3 Flory–Rehner theory

Flory–Rehner's theory has been applied in previous studies to describe the swelling behavior of microgels with temperature dependence.<sup>38,40,46,48</sup> The theory takes into account the contributions to osmotic pressure as mixing thermodynamics of polymer–solvent and the elasticity of the polymer network, which are given by:

$$\Pi_{\text{mix}} = -\frac{N_A k_B T}{v_S} [\ln(1 - \phi) + \phi + \chi\phi^2] \quad (1)$$

and

$$\Pi_{\text{el}} = -\frac{N_C k_B T}{V_0} \left[ \frac{\phi}{2\phi_0} - \left( \frac{\phi}{\phi_0} \right)^{1/3} \right]. \quad (2)$$

$N_C$  is the number of polymer chains in the network,  $\phi$  is the polymer volume fraction occupied by the polymer within the microgel volume,  $V_0$  is the volume of the microgel in the reference state, and  $\phi_0$  is the polymer volume fraction within the volume of the microgels in the reference state. Since the microgels are synthesized in bad solvent conditions, a natural choice for the reference state is the microgel in the collapsed state above the VPTT.<sup>4</sup>  $v_S$  is the molar volume of the solvent, and  $\chi$  is the Flory–Huggins interaction parameter.  $N_A$  is the

Avogadro's number. In thermodynamic equilibrium, the mixing and elastic contributions of the osmotic pressure are equal, which leads to eqn (3),<sup>46,69</sup> in which for a given temperature, the hydrodynamic radius of the microgel can be calculated.

$$\ln \left[ 1 - \phi_0 \left( \frac{R_{H,0}}{R_H} \right)^3 \right] + \phi_0 \left( \frac{R_{H,0}}{R_H} \right)^3 + \chi \phi_0^2 \left( \frac{R_{H,0}}{R_H} \right)^6 + \frac{\phi_0}{N_{\text{gel}}} \left( \frac{R_{H,0}}{R_H} - \frac{1}{2} \left( \frac{R_{H,0}}{R_H} \right)^3 \right) = 0. \quad (3)$$

$N_{\text{gel}} = (V_0 \phi_0 N_A) / (\nu_S N_C)$  is the number of segments between two crosslinking points and  $R_{H,0}$  is the hydrodynamic radius at the reference state.

#### 2.4 Flory–Huggins interaction parameter

The Flory–Huggins interaction parameter  $\chi$  can be expressed as a series expansion of temperature and volume fraction.<sup>70</sup> We choose the original expression<sup>71</sup> of  $\chi$  as we obtain a reasonable agreement between the experiments of this study and the model. By introducing higher order terms in  $\chi$ , additional free parameters are introduced, which makes the study of deuteration challenging. Therefore, in this study, the Flory–Huggins interaction parameter is defined as:

$$\chi = \frac{1}{2} - A \left( 1 - \frac{\Theta}{T} \right), \quad (4)$$

where the parameters  $\Theta$  and  $A$  are the characteristic temperature of the volume phase transition and a dimensionless parameter, respectively.

The changes in the values of  $\chi_{\text{qc}}^i$  upon deuteration are calculated from quantum mechanical methods. The  $i = \text{NIPAM-H}_2\text{O}$ ,  $\text{D}_7\text{NIPAM-H}_2\text{O}$  stands for the quantum mechanically predicted Flory–Huggins interaction parameter describing the NIPAM- and  $\text{D}_7\text{NIPAM}$ -based microgels in  $\text{H}_2\text{O}$ , respectively. The interaction parameter  $\chi_{\text{qc}}^i$  for both NIPAM- and  $\text{D}_7\text{NIPAM}$ -based microgels can be calculated as,

$$\chi_{\text{qc}}^i = \frac{\Delta G_{\text{SP}} - \frac{1}{2}(\Delta G_{\text{PP}} + \Delta G_{\text{SS}})}{RT}, \quad (5)$$

where  $\Delta G_{\text{SP}}$ ,  $\Delta G_{\text{PP}}$ , and  $\Delta G_{\text{SS}}$  is the Gibbs free energy when a solvent–polymer, polymer–polymer, and solvent–solvent contact occurs, respectively. Each term represents the absolute Gibbs free energy of the complex that is considered.

The electronic structures of NIPAM and  $\text{D}_7\text{NIPAM}$  remain the same, as the only difference is due to deuteration. To predict the change of  $\chi_{\text{qc}}^i$  from quantum mechanical methods, only the ZPEs are therefore considered. The change of the Flory–Huggins interaction parameter upon deuteration is given by (see ESI† for more details)

$$\Delta \chi_{\text{qc}} = \chi_{\text{qc}}^{\text{D}_7\text{NIPAM-H}_2\text{O}} - \chi_{\text{qc}}^{\text{NIPAM-H}_2\text{O}}. \quad (6)$$

It is known that the different C–H/D ZPEs result in different C–D and C–H bond lengths.<sup>72</sup> We neglect these effects similar to literature studies,<sup>61,62</sup> and thus, we assume that only the

vibrational frequencies and ZPEs differ within isotopically substituted bonds.

#### 2.5 Computational details

For each NIPAM– $(\text{H}_2\text{O})_n$ ,  $(\text{H}_2\text{O})_n$ , and NIPAM–NIPAM complexes, CREST<sup>73</sup> is used to identify the most stable conformer at the GFN2-xTB level of theory. The identified complexes are used as input and further optimized at B3LYP<sup>74</sup> method with TZVP<sup>75</sup> basis set as well as D3BJ dispersion correction<sup>76</sup> with the software GAUSSIAN. At the same level of theory, the vibrational frequency calculations are performed, and the rigid rotor harmonic oscillator (RRHO) model is used to obtain the ZPEs. The B3LYP method is known to give accurate equilibrium geometries<sup>77–79</sup> and very accurate frequencies with a root mean square error of  $31 \text{ cm}^{-1}$  (ref. 80) at a low computational cost. We approximate the  $\Delta G_{\text{PP}}$  term of the NIPAM–NIPAM interactions by considering only two NIPAM monomers. For the  $\Delta G_{\text{SP}}$  and  $\Delta G_{\text{PP}}$  terms, we increase the number of  $\text{H}_2\text{O}$  molecules until the  $\Delta \chi_{\text{qc}}$  is converged. Electronic structures and geometries remain identical for the hydrogenated and deuterated complexes. Therefore, for the deuterated complexes, only vibrational frequency calculations are repeated using the force constants from the hydrogenated complexes' calculations.

### 3 Results and discussion

#### 3.1 Study of NIPAM/D<sub>7</sub>NIPAM– $(\text{H}_2\text{O})_n$ complexes

The change of the Flory–Huggins interaction parameter upon deuteration in units of  $RT$ , where  $R$  is the gas constant and  $T$  is the temperature, against the number of  $\text{H}_2\text{O}$  molecules for different NIPAM/D<sub>7</sub>NIPAM– $(\text{H}_2\text{O})_n$  complexes is shown in Fig. 1.

For  $n = 1$ , a hydrogen bond occurs between the H of  $\text{H}_2\text{O}$  and the O=C of the NIPAM monomer due to oxygen's high

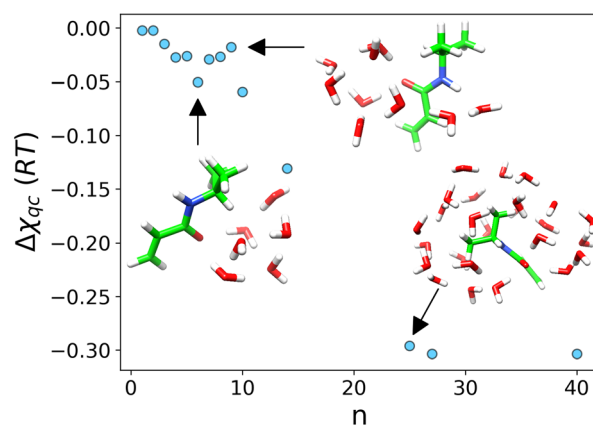


Fig. 1 The change of Flory–Huggins interaction parameter  $\Delta \chi_{\text{qc}}$  due to deuteration against NIPAM (carbon atoms in green) with the number of  $\text{H}_2\text{O}$  molecules (red and white). Hydration takes place first at the oxygen atom (red), second at the nitrogen atom (blue) and last, at the isopropyl group.

electronegativity. To study the effect of individual hydrogen bonds on oxygen and nitrogen of NIPAM, we manually transfer the  $\text{H}_2\text{O}$  molecule in the vicinity of nitrogen. We find that  $\Delta\chi_{\text{qc}}$  takes the values  $-0.002(RT)$  (increase of VPTT) and  $0.04(RT)$  (decrease of VPTT) for the hydrogen bonds  $\text{H}\cdots\text{O}=\text{C}$  and  $\text{H}\cdots\text{N}-\text{H}$ , respectively.

Increasing the number of  $\text{H}_2\text{O}$  molecules to take both hydrogen bonds with opposing effects into account (up to  $n = 8$ ),  $\Delta\chi_{\text{qc}}$  decreases till it reaches a local minimum for  $n = 6$  and increases again till  $n = 8$ . For  $n = 6$ , the NIPAM/D<sub>7</sub>NIPAM (carbon atoms in green) with  $(\text{H}_2\text{O})_6$  (red and white) are shown in the left of Fig. 1. Two  $\text{H}_2\text{O}$  molecules create hydrogen bonds with the oxygen atom of the NIPAM monomer. For  $n = 9$ , the most energetically stable NIPAM/D<sub>7</sub>NIPAM- $(\text{H}_2\text{O})_9$  complex geometry that we obtain is shown in the top-right of Fig. 1 with  $\Delta\chi_{\text{qc}} = -0.018t(RT)$ . One of nine  $\text{H}_2\text{O}$  molecules creates a hydrogen bond with the nitrogen atom of NIPAM. After oxygen, nitrogen is the most electronegative atom and thus, a hydrogen bond  $\text{H}\cdots\text{N}-\text{H}$  is expected. For values larger than 9, the  $\Delta\chi_{\text{qc}}$  decreases with the increase of  $n$ , which results in a higher shift of VPTT.

To further study the hydration of and the effect of deuteration, we add more  $\text{H}_2\text{O}$  molecules to hydrate the isopropyl group. For  $n = 14$ , the isopropyl group is only partially hydrated. The value of  $\Delta\chi_{\text{qc}}$  decreases to  $-0.13(RT)$ , which indicates that the isotope effect is more substantially observable. Only for 25  $\text{H}_2\text{O}$  molecules, the isopropyl group is fully hydrated, which results in  $\Delta\chi_{\text{qc}} = -0.29(RT)$ . The most stable geometry of NIPAM- $(\text{H}_2\text{O})_{25}$  complex is shown in bottom-right of Fig. 1. For this geometry,  $\text{H}_2\text{O}$  molecules create hydrogen bonds with the oxygen and nitrogen atoms and have van der Waals interactions with the isopropyl group.

To fully characterize the isotope effect, the isopropyl group needs to be hydrated and this happens only when both oxygen and nitrogen atoms are hydrated. We perform calculations for  $n = 27$  and  $n = 40$ , in order to check how  $\Delta\chi_{\text{qc}}$  changes its value by adding more  $\text{H}_2\text{O}$  molecules. Both for  $n = 27$  and  $n = 40$ ,  $\Delta\chi_{\text{qc}}$  changes its value only by 2% which indicates that the result has converged. For this reason, we conclude that 25  $\text{H}_2\text{O}$  molecules are appropriate for studying the deuteration effect.

### 3.2 Swelling of microgels

In Fig. 2, the circles and triangles represent the values of the hydrodynamic radii obtained from multi-angle DLS,  $R_{\text{H}}$ , as a function of the temperature  $T$ , for the pNIPAM and pD<sub>7</sub>NIPAM microgels, respectively. The calculated values for the hydrodynamic radius are plotted as lines.

Eqn (3) and (4) (Flory–Huggins interaction parameter) are fitted (straight line and dashed line) against the experimental data (circles and triangles) of the pNIPAM and pD<sub>7</sub>NIPAM microgels, respectively. In general, a reasonable fit is obtained for the swelling curves of pNIPAM and pD<sub>7</sub>NIPAM microgels with a coefficient of determination ( $R^2$ ) of 0.99 and 0.96, respectively.

For the pNIPAM microgel, in the  $20\text{ }^{\circ}\text{C} \leq T \leq 25\text{ }^{\circ}\text{C}$  and  $48\text{ }^{\circ}\text{C} \leq T \leq 50\text{ }^{\circ}\text{C}$  range, the Flory–Huggins theory slightly

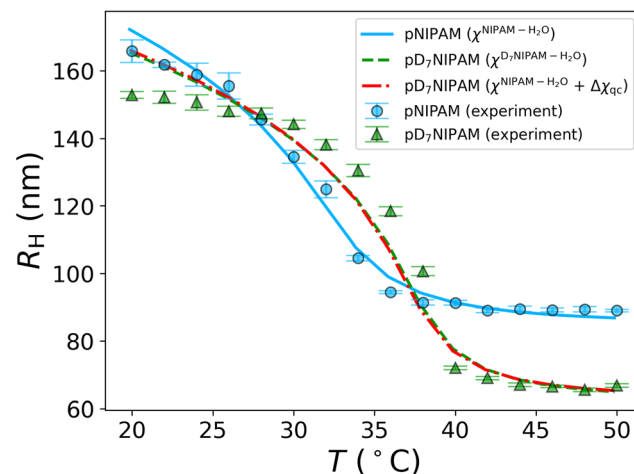


Fig. 2 Measured (circles, triangles) and fitted (straight line, dashed line) hydrodynamic radius  $R_{\text{H}}$  of pNIPAM and pD<sub>7</sub>NIPAM microgels in  $\text{H}_2\text{O}$  over temperature  $T$ . To estimate the swelling curve of the pD<sub>7</sub>NIPAM microgel (dashdot line), the quantum mechanical predicted  $\Delta\chi_{\text{qc}}$  is added to the Flory–Huggins parameter  $\chi_{\text{qc}}^{\text{NIPAM}-\text{H}_2\text{O}}$  of the pNIPAM microgel in  $\text{H}_2\text{O}$ .

overestimates and underestimates the hydrodynamic radius, respectively. This is known in the literature<sup>46</sup> and it is due to the Flory–Huggins interaction parameter. Once more, it is important to note that the Flory–Rehner model can successfully describe the thermodynamic and mechanical parameters of pNIPAM microgels. However, studies have shown that unrealistic values for several fit parameters are required in order to obtain close agreement between the theory and experimental data for equilibrium swelling of microgels.<sup>48</sup>

Nonetheless, as the purpose of this work is to study the deuteration effect at a fundamental level, we conclude that the current choice of the Flory–Huggins interaction parameter given by eqn (4) leads to a reasonable fit and can describe the observed swelling behavior. A similar behavior is observed for the D<sub>7</sub>NIPAM microgel. In the  $20\text{ }^{\circ}\text{C} \leq T \leq 27\text{ }^{\circ}\text{C}$  and  $30\text{ }^{\circ}\text{C} \leq T \leq 37\text{ }^{\circ}\text{C}$  range, the Flory–Huggins theory overestimates and underestimates the hydrodynamic radius, respectively. During the fitting procedure, all four parameters ( $A$ ,  $\Theta$ ,  $N_{\text{gel}}$ , and  $\varphi_0$ ) are free to change. The resulting values of the fitting parameters are shown in Table 1 for both microgels.

Table 1 Fitted parameters of pNIPAM and pD<sub>7</sub>NIPAM microgels using the Flory–Huggins theory. For the pD<sub>7</sub>NIPAM<sup>†</sup>, the parameters  $A$  and  $\Theta$  are fixed to the corresponding fitted pNIPAM values while  $N_{\text{gel}}$  and  $\varphi_0$  are set free for optimization. Furthermore, quantum mechanically predicted  $\Delta\chi_{\text{qc}}$  is added to the  $\chi_{\text{qc}}^{\text{NIPAM}-\text{H}_2\text{O}}$  to compute the swelling behavior of pD<sub>7</sub>NIPAM microgel. The VPTT shifts by 4.9 K

Parameters	pNIPAM	pD <sub>7</sub> NIPAM	pD <sub>7</sub> NIPAM <sup>†</sup>
$A$	-30.9	-29.5	-30.9 (fixed)
$\Theta$ (°C)	32.2	37.1	32.2 (fixed)
$N_{\text{gel}}$	19.9	59.7	57.4
$\varphi_0$	0.88	0.82	0.84

After optimization, the dimensionless parameter  $A$  has a value of  $-30.9$  and  $-29.5$  for pNIPAM and pD<sub>7</sub>NIPAM microgels, respectively. Literature studies<sup>46,48,81–83</sup> report  $A$  in the range of  $-43.3 \leq A \leq -2$ . The fitted temperature  $\Theta$  is found =  $32.2$  °C and  $37.1$  °C in the case of pNIPAM and pD<sub>7</sub>NIPAM microgels, respectively, with a VPTT shift of  $4.9$  K. The calculated values of  $\Theta$  deviate  $1.9$  K and  $1.3$  K from the experimental values with a VPTT shift of  $4.3$  K, which are determined by fitting the sigmoid function to the measurements (see ESI†). For the pNIPAM microgel,  $N_{\text{gel}}$  is found  $19.9$ . Friesen *et al.*<sup>69</sup> shows that  $N_{\text{gel}} = 10$  for microgels with comparable but homogeneously distributed amount of crosslinks. Our values therefore indicate that that BIS is not homogeneously distributed inside the microgel. This is in agreement with the experimental structure of microgels probed using both scattering<sup>4,5,29,39</sup> and microscopy techniques<sup>10,11,84</sup> which shows a decreasing crosslinks concentration from the core to the microgel periphery.

For the pD<sub>7</sub>NIPAM microgel,  $N_{\text{gel}}$  is found  $59.7$ . This larger value of  $N_{\text{gel}}$  compared to pNIPAM microgel value results by definition of  $N_{\text{gel}}$  into less amount of BIS incorporated into the microgel. The volume fraction of the polymer  $\varphi_0$  has a value of  $0.88$  and  $0.82$  for the pNIPAM and pD<sub>7</sub>NIPAM microgels, respectively. From the fitting, we obtain a standard error of  $1\sigma = 0.06$  for  $\varphi_0$ . The  $\varphi_0$  values which we obtain in this work are consistent with measurements<sup>85–87</sup> and theoretical studies<sup>46</sup> of  $\varphi_0 = 0.7$  and  $\varphi_0 = 0.84$ , respectively. However, this is still debated since, as reported by Lopez *et al.*<sup>48</sup>  $\varphi_0 = 0.44$  is also reasonable. The parameter  $\varphi_0$  is in the range of  $0.44 \leq \varphi_0 \leq 0.85$  with an average value of  $0.8$ . Using an approximation based on viscosimetry measurements and DLS (see ESI†), we estimate  $\varphi_0 = 0.58 \pm 0.06$  and  $\varphi_0 = 0.51 \pm 0.03$  for the pNIPAM and pD<sub>7</sub>NIPAM microgels, respectively. As a result, the simulated and approximated  $\varphi_0$  agrees only within the  $4\sigma$  standard deviation. However, this derivation is based on an approximation and in this work, we obtain best fits for the parameter values shown in Table 1.

As described in detail in the previous section, the change of the Flory–Huggins interaction parameter upon deuteration  $\Delta\chi_{\text{qc}}$  is obtained by eqn (6) with quantum chemical calculations. Next,  $\Delta\chi_{\text{qc}}$  is added to  $\chi^{\text{NIPAM-H}_2\text{O}}$  to predict the swelling curve of pD<sub>7</sub>NIPAM microgel. During the calculation, the parameters  $A$  and  $\Theta$  are fixed to the value determined from the pNIPAM microgel while the parameters  $\varphi_0$  and  $N_{\text{gel}}$  are set free for optimization. The resulting parameters are shown in Table 1. After optimization, we obtain a value of  $\varphi_0 = 0.84$ . The value of the  $N_{\text{gel}}$  for the pD<sub>7</sub>NIPAM microgel is increased compared to the pNIPAM microgel. This might be explained by the absence of self-crosslinking for the D<sub>7</sub>NIPAM-based microgel,<sup>34</sup> resulting to longer polymer chains between two crosslinking points. For both  $\varphi_0$  and  $N_{\text{gel}}$  parameters, similar values are obtained from the FR theory + $\Delta\chi_{\text{qc}}$  compared to FR theory in the case of pD<sub>7</sub>NIPAM microgel. The resulting swelling curve of the pD<sub>7</sub>NIPAM microgel is shown in Fig. 2 and agrees with the measured swelling curve with a coefficient of determination ( $R^2$ ) of  $0.96$ . Based on our results, the VPTT shifts by

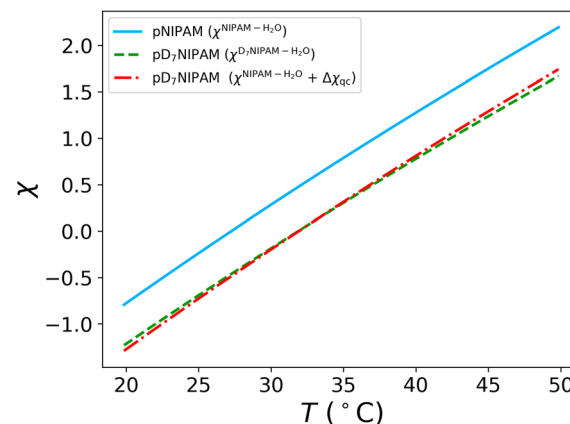


Fig. 3 Flory–Huggins interaction parameter  $\chi$  fitted to experimental data NIPAM (straight line) and D<sub>7</sub>NIPAM (dashed line) microgels using FR theory. The Flory–Huggins interaction parameter of D<sub>7</sub>NIPAM is calculated (dashdot line) by adding the predicted change  $\Delta\chi_{\text{qc}}$  from quantum mechanics due to deuteration to  $\chi^{\text{NIPAM-H}_2\text{O}}$ .

$4.9$  K, similar to the value which is obtained by just using the FR model. In the  $20$  °C  $\leq T \leq 25$  °C and  $28$  °C  $\leq T \leq 36$  °C range, our approach overestimates and underestimates the swelling behavior of the pD<sub>7</sub>NIPAM microgel.

In Fig. 3, the Flory interaction parameter  $\chi$  in the case of pNIPAM (straight line) and pD<sub>7</sub>NIPAM (dashed line) microgels obtained by FR theory is shown, respectively. The Flory parameter of the pD<sub>7</sub>NIPAM microgel (dashdot line) calculated from eqn (4) and (6) for  $n = 25$  is also shown in Fig. 3. For the temperature range between  $20$ – $50$  °C, the  $\chi^{\text{NIPAM-H}_2\text{O}}$  of NIPAM-based microgel is always larger than the  $\chi^{\text{D}^7\text{NIPAM-H}_2\text{O}}$  of D<sub>7</sub>NIPAM-based microgel with maximum difference ( $\chi^{\text{D}^7\text{NIPAM-H}_2\text{O}} - \chi^{\text{NIPAM-H}_2\text{O}}$ ) of  $-0.5$  at  $T = 20$  °C. That means that the Gibbs free energy difference is higher in the case of NIPAM-based microgel in H<sub>2</sub>O favoring the demixing compared to D<sub>7</sub>NIPAM-based microgel.

## 4 Conclusions

In this work, we studied experimentally and computationally the deuteration effect on pNIPAM microgels. To do so, pD<sub>7</sub>NIPAM microgel was used as a case study due to its large VPTT shift compared to pNIPAM microgel.

Using quantum mechanical methods, we investigated different NIPAM-(H<sub>2</sub>O)<sub>n</sub> complexes with  $n$  being the number of H<sub>2</sub>O molecules and calculated the change in the value of the Flory–Huggins interaction parameter as a consequence of deuteration. We found that a complex of NIPAM with at least  $25$  H<sub>2</sub>O molecules is necessary to study the effect of deuteration. For this number of H<sub>2</sub>O molecules, the isopropyl group of NIPAM is fully hydrated.

The Flory–Rehner theory was used to model the swelling curve of pNIPAM and pD<sub>7</sub>NIPAM microgels. First, we fit the data of pNIPAM and pD<sub>7</sub>NIPAM microgels, leaving all the parameters of the model free to change. In both cases, reason-

able fits and values of the fitting parameters in agreement with the literature were obtained. From these fits, we also estimate the shift in the VPTT due to the deuteration is  $\approx 4.3$  K. We also note that this shift of the VPTT is consistent with the shift obtained starting from the value of  $\chi$  for pNIPAM as obtained from the fit and adding the  $\Delta\chi_{qc}$  we compute. Then, we modeled the swelling behavior of the pD<sub>7</sub>NIPAM microgel, by fixing the parameters  $A$  and  $\Theta$  to the values found from the fitting of the pNIPAM microgel, and we optimized the parameters  $N_{gel}$  and  $\varphi_0$  based on the experimental results of pD<sub>7</sub>NIPAM microgel. During the optimization, the resulting change of the Flory-Huggins interaction parameter upon deuteration  $\Delta\chi_{qc}$  from the *ab initio* calculations was incorporated in the Flory-Rehner theory. We found that  $N_{gel}$  is larger in the case of pD<sub>7</sub>NIPAM microgel, which may be due to the suppression of the self-crosslinking due to the use of D<sub>7</sub>NIPAM as monomer.<sup>34</sup> The volume fraction of the polymer  $\varphi_0$  has a smaller value in the case of pD<sub>7</sub>NIPAM microgel.

In the future, our approach may be applied to the adjustment of effective parameters in molecular dynamics simulations for the study of deuterated microgels.<sup>8,39,88</sup> This will provide insights into properties such as VPTT, swelling ratio, and softness.

## Data availability

All optimized molecular geometries and multi-angle dynamic light scattering measurements have been deposited in the RADAR4Chem database under doi (<https://doi.org/10.22000/857>).

## Conflicts of interest

There are no conflicts to declare.

## Acknowledgements

The authors gratefully acknowledge financial support from the SFB 985 Functional Microgels and Microgel Systems of Deutsche Forschungsgemeinschaft (DFG, German Research Foundation). Simulations were performed with computing resources granted by RWTH Aachen University under project rwth0739. Molecular graphics in Fig. 1 performed with UCSF Chimera.

## References

- 1 P. N. Pusey and W. Van Megen, *Nature*, 1986, **320**, 340–342.
- 2 U. Gasser, E. R. Weeks, A. Schofield, P. Pusey and D. Weitz, *Science*, 2001, **292**, 258–262.
- 3 M. Karg, A. Pich, T. Hellweg, T. Hoare, L. A. Lyon, J. Crassous, D. Suzuki, R. A. Gumerov, S. Schneider, I. I. Potemkin, *et al.*, *Langmuir*, 2019, **35**, 6231–6255.
- 4 A. Scotti, M. F. Schulte, C. G. Lopez, J. J. Crassous, S. Bochenek and W. Richtering, *Chem. Rev.*, 2022, **122**, 11675–11700.
- 5 M. Stieger, W. Richtering, J. S. Pedersen and P. Lindner, *J. Chem. Phys.*, 2004, **120**, 6197–6206.
- 6 M. Cors, L. Wiehemeier, Y. Hertle, A. Feoktystov, F. Cousin, T. Hellweg and J. Oberdisse, *Langmuir*, 2018, **34**, 15403–15415.
- 7 A. Scotti, J. Houston, M. Brugnoni, M. Schmidt, M. Schulte, S. Bochenek, R. Schweins, A. Feoktystov, A. Radulescu and W. Richtering, *Phys. Rev. E*, 2020, **102**, 052602.
- 8 N. Gnan, L. Rovigatti, M. Bergman and E. Zaccarelli, *Macromolecules*, 2017, **50**, 8777–8786.
- 9 A. Scotti, *Soft Matter*, 2021, **17**, 5548–5559.
- 10 G. M. Conley, P. Aebischer, S. Nöjd, P. Schurtenberger and F. Scheffold, *Sci. Adv.*, 2017, **3**, e1700969.
- 11 G. M. Conley, C. Zhang, P. Aebischer, J. L. Harden and F. Scheffold, *Nat. Commun.*, 2019, **10**, 2436.
- 12 A. Scotti, M. Pelaez-Fernandez, U. Gasser and A. Fernandez-Nieves, *Phys. Rev. E*, 2021, **103**, 012609.
- 13 M. Heskins and J. E. Guillet, *J. Macromol. Sci., Chem.*, 1968, **2**, 1441–1455.
- 14 R. Pelton and P. Chibante, *Colloids Surf.*, 1986, **20**, 247–256.
- 15 D. Menne, F. Pitsch, J. E. Wong, A. Pich and M. Wessling, *Angew. Chem., Int. Ed.*, 2014, **53**, 5706–5710.
- 16 W. Richtering, *Langmuir*, 2012, **28**, 17218–17229.
- 17 F. A. Plamper and W. Richtering, *Acc. Chem. Res.*, 2017, **50**, 131–140.
- 18 J. Brijitta and P. Schurtenberger, *Curr. Opin. Colloid Interface Sci.*, 2019, **40**, 87–103.
- 19 H. Senff and W. Richtering, *J. Chem. Phys.*, 1999, **111**, 1705–1711.
- 20 J. Mattsson, H. M. Wyss, A. Fernandez-Nieves, K. Miyazaki, Z. Hu, D. R. Reichman and D. A. Weitz, *Nature*, 2009, **462**, 83–86.
- 21 M. Deloney, K. Smart, B. A. Christiansen and A. Panitch, *J. Controlled Release*, 2020, **323**, 47–58.
- 22 W. Richtering, I. Alberg and R. Zentel, *Small*, 2020, **16**, 2002162.
- 23 E. Miceli, B. Kuropka, C. Rosenauer, E. R. Osorio Blanco, L. E. Theune, M. Kar, C. Weise, S. Morsbach, C. Freund and M. Calderón, *Nanomedicine*, 2018, **13**, 2657–2668.
- 24 A. Scotti, A. R. Denton, M. Brugnoni, J. E. Houston, R. Schweins, I. I. Potemkin and W. Richtering, *Macromolecules*, 2019, **52**, 3995–4007.
- 25 U. Gasser, J. Hyatt, J.-J. Lietor-Santos, E. Herman, L. A. Lyon and A. Fernandez-Nieves, *J. Chem. Phys.*, 2014, **141**, 034901.
- 26 P. S. Mohanty, S. Nöjd, K. v. Gruijthuijsen, J. J. Crassous, M. Obiols-Rabasa, R. Schweins, A. Stradner and P. Schurtenberger, *Sci. Rep.*, 2017, **7**, 1487.
- 27 S. Nöjd, P. Holmqvist, N. Boon, M. Obiols-Rabasa, P. S. Mohanty, R. Schweins and P. Schurtenberger, *Soft Matter*, 2018, **14**, 4150–4159.
- 28 M. Cors, L. Wiehemeier, O. Wrede, A. Feoktystov, F. Cousin, T. Hellweg and J. Oberdisse, *Soft Matter*, 2020, **16**, 1922–1930.

29 J. E. Houston, L. Fruhner, A. de la Cotte, J. Rojo González, A. V. Petrunin, U. Gasser, R. Schweins, J. Allgaier, W. Richtering, A. Fernandez-Nieves, *et al.*, *Sci. Adv.*, 2022, **8**, eabn6129.

30 F. S. Varley, *Neutron News*, 1992, **3**, 29–37.

31 A. Scotti, U. Gasser, B. Zhou, A. Arenas-Gullo, A. de la Cotte, J. R. González and A. Fernandez-Nieves, in *Compressible Microgels in Concentrated Suspensions: Phase Behavior, Flow Properties, and Scattering Techniques to Probe Their Structure and Dynamics*, John Wiley & Sons, Ltd, 2022, ch. 6, pp. 203–240.

32 M. Brugnoni, A. Scotti, A. A. Rudov, A. P. Gelissen, T. Caumanns, A. Radulescu, T. Eckert, A. Pich, I. I. Potemkin and W. Richtering, *Macromolecules*, 2018, **51**, 2662–2671.

33 A. J. Schmid, J. Dubbert, A. A. Rudov, J. S. Pedersen, P. Lindner, M. Karg, I. I. Potemkin and W. Richtering, *Sci. Rep.*, 2016, **6**, 1–13.

34 M. Brugnoni, A. C. Nickel, L. C. Kröger, A. Scotti, A. Pich, K. Leonhard and W. Richtering, *Polym. Chem.*, 2019, **10**, 2397–2405.

35 T. Widmann, L. P. Kreuzer, N. Hohn, L. Bießmann, K. Wang, S. Rinner, J.-F. Moulin, A. J. Schmid, Y. Hannappel, O. Wrede, *et al.*, *Langmuir*, 2019, **35**, 16341–16352.

36 H. Shirota, N. Kuwabara, K. Ohkawa and K. Horie, *J. Phys. Chem. B*, 1999, **103**, 10400–10408.

37 M. Cors, L. Wiehemeier, J. Oberdisse and T. Hellweg, *Polymers*, 2019, **11**(4), 620.

38 M. Urich and A. R. Denton, *Soft Matter*, 2016, **12**, 9086–9094.

39 N. Boon and P. Schurtenberger, *Phys. Chem. Chem. Phys.*, 2017, **19**, 23740–23746.

40 T. J. Weyer and A. R. Denton, *Soft Matter*, 2018, **14**, 4530–4540.

41 P. J. Flory, *Principles of Polymer Chemistry*, Cornell University Press, Ithaca, 1953.

42 P. J. Flory and J. Rehner, *J. Chem. Phys.*, 1943, **11**, 512–520.

43 P. J. Flory and J. Rehner, *J. Chem. Phys.*, 1943, **11**, 521–526.

44 L. D. Landau and E. M. Lifshitz, *Theory of Elasticity*, Elsevier, Amsterdam, 3rd edn, 1986.

45 J.-J. Lietor-Santos, B. Sierra-Martin, R. Vavrin, Z. Hu, U. Gasser and A. Fernandez-Nieves, *Macromolecules*, 2009, **42**, 6225–6230.

46 S. Friesen, Y. Hannappel, S. Kakorin and T. Hellweg, *Colloid Polym. Sci.*, 2022, **300**, 1235–1245.

47 P. Voudouris, D. Florea, P. van der Schoot and H. M. Wyss, *Soft Matter*, 2013, **9**, 7158–7166.

48 C. G. Lopez and W. Richtering, *Soft Matter*, 2017, **13**, 8271–8280.

49 F. A. L. Janssen, M. Kather, L. C. Kröger, A. Mhamdi, K. Leonhard, A. Pich and A. Mitsos, *Ind. Eng. Chem. Res.*, 2017, **56**, 14545–14556.

50 F. A. Janssen, A. Ksiazkiewicz, M. Kather, L. C. Kröger, A. Mhamdi, K. Leonhard, A. Pich and A. Mitsos, *28th European Symposium on Computer Aided Process Engineering*, Elsevier, 2018, vol. 43, pp. 109–114.

51 F. Jung, F. A. L. Janssen, A. Ksiazkiewicz, A. Caspari, A. Mhamdi, A. Pich and A. Mitsos, *Ind. Eng. Chem. Res.*, 2019, **58**, 13675–13685.

52 S. Schneider, F. Jung, O. Mergel, J. Lammertz, A. C. Nickel, T. Caumanns, A. Mhamdi, J. Mayer, A. Mitsos and F. A. Plamper, *Polym. Chem.*, 2020, **11**, 315–325.

53 L. C. Kröger, W. A. Kopp and K. Leonhard, *J. Phys. Chem. B*, 2017, **121**, 2887–2895.

54 P. Deglmann, I. Müller, F. Becker, A. Schäfer, K.-D. Hungenberg and H. Weiss, *Macromol. React. Eng.*, 2009, **3**, 496–515.

55 M. L. Coote, *Macromol. Theory Simul.*, 2009, **18**, 388–400.

56 T. Nevolianis, N. Wolter, L. F. Kaven, L. Krep, C. Huang, A. Mhamdi, A. Mitsos, A. Pich and K. Leonhard, *Ind. Eng. Chem. Res.*, 2023, **62**, 893–902.

57 M. Ceriotti and T. E. Markland, *J. Chem. Phys.*, 2013, **138**, 014112.

58 M. Gómez-Gallego and M. A. Sierra, *Chem. Rev.*, 2011, **111**, 4857–4963.

59 K. Świderek and P. Paneth, *Chem. Rev.*, 2013, **113**, 7851–7879.

60 K. Karandashev, Z.-H. Xu, M. Meuwly, J. Vaníček and J. O. Richardson, *Struct. Dyn.*, 2017, **4**, 061501.

61 J. S. Mugridge, R. G. Bergman and K. N. Raymond, *J. Am. Chem. Soc.*, 2012, **134**, 2057–2066.

62 C. L. Perrin and P. Karri, *J. Am. Chem. Soc.*, 2010, **132**, 12145–12149.

63 A. Scotti, U. Gasser, E. S. Herman, M. Pelaez-Fernandez, J. Han, A. Menzel, L. A. Lyon and A. Fernández-Nieves, *Proc. Natl. Acad. Sci. U. S. A.*, 2016, **113**, 5576–5581.

64 S. Fujishige, K. Kubota and I. Ando, *J. Phys. Chem.*, 1989, **93**, 3311–3313.

65 M. Andersson and S. L. Maunu, *J. Polym. Sci., Part B: Polym. Phys.*, 2006, **44**, 3305–3314.

66 D. E. Koppel, *J. Chem. Phys.*, 1972, **57**, 4814–4820.

67 W. Burchard and W. Richtering, *Prog. Colloid Polym. Sci.*, 1989, **80**, 151–163.

68 A. e. Scotti, W. Liu, J. Hyatt, E. Herman, H. Choi, J. Kim, L. Lyon, U. Gasser and A. Fernandez-Nieves, *J. Chem. Phys.*, 2015, **142**, 234905.

69 S. Friesen, Y. Hannappel, S. Kakorin and T. Hellweg, *Gels*, 2021, **7**(2), 42.

70 B. Erman and P. J. Flory, *Macromolecules*, 1986, **19**, 2342–2353.

71 P. J. Flory and J. Rehner, *J. Chem. Phys.*, 1943, **11**, 512–520.

72 J. Mugridge, R. Bergman and K. Raymond, *Angew. Chem., Int. Ed.*, 2010, **49**, 3635–3637.

73 P. Pracht, F. Bohle and S. Grimme, *Phys. Chem. Chem. Phys.*, 2020, **22**, 7169–7192.

74 P. Stephens, F. Devlin, C. Chabalowski and M. J. Frisch, *J. Phys. Chem.*, 1994, **98**, 11623–11627.

75 A. Schäfer, C. Huber and R. Ahlrichs, *J. Chem. Phys.*, 1994, **100**, 5829–5835.

76 S. Grimme, *J. Comput. Chem.*, 2006, **27**, 1787–1799.

77 J. A. Montgomery, M. J. Frisch, J. W. Ochterski and G. A. Petersson, *J. Chem. Phys.*, 1999, **110**, 2822–2827.

78 L. A. Curtiss, P. C. Redfern, K. Raghavachari and J. A. Pople, *J. Chem. Phys.*, 2001, **114**, 108–117.

79 J. Zheng, Y. Zhao and D. G. Truhlar, *J. Chem. Theory Comput.*, 2009, **5**, 808–821.

80 J. P. Merrick, D. Moran and L. Radom, *J. Phys. Chem. A*, 2007, **111**, 11683–11700.

81 Y. Hertle, M. Zeiser, C. Hasenöhrl, P. Busch and T. Hellweg, *Colloid Polym. Sci.*, 2010, **288**, 1047–1059.

82 V. Nigro, R. Angelini, M. Bertoldo and B. Ruzicka, *Colloids Surf. A*, 2017, **532**, 389–396.

83 T. López-León and A. Fernández-Nieves, *Phys. Rev. E: Stat., Nonlinear, Soft Matter Phys.*, 2007, **75**, 011801.

84 M. F. Schulte, S. Bochenek, M. Brugnoni, A. Scotti, A. Mourran and W. Richtering, *Angew. Chem., Int. Ed.*, 2021, **60**, 2280–2287.

85 G. Romeo, L. Imperiali, J.-W. Kim, A. Fernández-Nieves and D. A. Weitz, *J. Chem. Phys.*, 2012, **136**, 124905.

86 M. Reufer, P. Diaz-Leyva, I. Lynch and F. Scheffold, *Eur. Phys. J. E: Soft Matter Biol. Phys.*, 2009, **28**, 165–171.

87 A. K. Lele, M. M. Hirve, M. V. Badiger and R. A. Mashelkar, *Macromolecules*, 1997, **30**, 157–159.

88 S. V. Nikolov, A. Fernandez-Nieves and A. Alexeev, *Proc. Natl. Acad. Sci. U. S. A.*, 2020, **117**, 27096–27103.